

NUMERICAL AND EXPERIMENTAL INVESTIGATION OF LINER TOP THICKNESS ON THE FORMATION AND PENETRATION PERFORMANCE OF EXPLOSIVELY FORMED PROJECTILES

Pham Hong Quan^{✉,*}, Do Van Minh[✉], Tran Dinh Thanh

Le Quy Don Technical University, 236 Hoang Quoc Viet, Hanoi, Vietnam

*E-mail: phquanstudying@lqdtu.edu.vn

Received: 16 July 2025 / Revised: 29 September 2025 / Accepted: 01 October 2025

Published online: 04 November 2025

Abstract. This paper presents a detailed investigation, both numerical and experimental, into the influence of liner top thickness (denoted as δ_1) on the formation dynamics and terminal performance of explosively formed projectiles (EFPs). Six structural variants of a 54 mm caliber EFP warhead were modeled using Ansys Autodyn, with top thickness-to-diameter ratios (δ_1/d) ranging from 0.02 to 0.07. The simulations evaluated key performance metrics, including projectile velocity, kinetic energy distribution, penetration depth, and cavity dimensions. Results demonstrated that EFPs with δ_1/d between 0.03 and 0.05 achieved the best overall balance between aerodynamic stability, structural coherence, and penetration effectiveness. Experimental validation for a configuration with $\delta_1 = 2$ mm ($\delta_1/d \approx 0.044$) showed good agreement in both velocity and cavity geometry. These findings provide robust design guidelines for optimizing EFP liners and confirm the reliability of numerical modeling for preliminary engineering evaluations.

Keywords: explosively formed projectile, liner thickness, numerical simulation, penetration depth, Ansys Autodyn.

1. INTRODUCTION

Explosively formed projectile (EFP) is a type of projectile that uses the principle of concentrated explosive energy designed to produce high-velocity projectiles capable of penetrating armor at long standoff distances. Their formation is governed by a complex interplay of detonation waves, liner geometry, and material response under extreme strain rates. Among various design parameters, the geometry and thickness distribution

of the metallic liner play a pivotal role in determining the projectile's shape, velocity, and ultimately its penetration capability.

Previous studies have primarily focused on the effects of liner shape (e.g., hemispherical, conical) and explosive charge configurations. However, limited attention has been paid to the influence of liner top thickness (δ_1), especially when considering non-uniform, radially varying thickness profiles. A thicker top may enhance structural integrity but also resist axial collapse, thereby reducing forward momentum. Conversely, a thinner top may result in higher velocities but lead to instability and aerodynamic inefficiency.

Several previous studies have highlighted the significant influence of liner thickness on the formation and performance of EFPs. Cardoso showed that for uniform liners, optimal velocity and kinetic energy are achieved when the thickness is 4–7% of the liner diameter [1]. Yang's study validated numerical simulations with experimental results, reporting velocity errors below 5% and showing that non-uniform liners yield more stable and higher EFP velocities [2]. Minh and colleagues studied the influence of the curvature radius structure of the liner on the velocity and penetration ability of EFP by numerical simulation method and the error compared with the experimental results was less than 8% [3]. Quan et al. studied the effect of the liner height and found that the liner height of 0.2–0.3 times the liner diameter gave EFP a good aerodynamic shape, achieving high velocity and large penetration depth [4]. Salkičević confirmed that decreasing liner thickness improves EFP energy, and that liners tapering from top to base outperform the opposite [5]. Wu et al. proposed a preliminary structure of the liner and explosive charge [6]. Couque conducted experiments and recommended using Ansys Autodyn software with a modified Johnson-Cook (MJC) model for smaller error compared to the Johnson-Cook (JC) model [7–9]. These studies confirm that liner thickness plays a critical role in EFP performance. While recommended ranges for uniform liners have been proposed, detailed studies of non-uniform configurations are still limited.

This study addresses this issue by investigating the effect of δ_1 variations on projectile formation, velocity, energy distribution, and penetration capacity. The work integrates numerical simulations using Ansys Autodyn with full-scale experimental validation to generate a comprehensive design framework.

2. MATERIAL AND METHODS

2.1. Geometric Model and Calculation Method

The study focuses on a 54 mm EFP warhead shown in Fig. 1. The warhead includes four main components: the casing, explosive charge, detonator, and liner. The liner, made

of oxygen-free high-conductivity (OFHC) copper, has a hemispherical profile characterized by its height h , diameter d , outer radius r_1 , and inner radius r_2 . The liner also includes a top thickness δ_1 , an edge thickness δ_2 , and two geometric offsets: X_1 and X_2 , which represent the distances from the centers of the outer and inner radii, respectively, to the bottom of the warhead along the axis of symmetry (OX). The casing, constructed from polyethylene plastic, is designed as a cylindrical shell with an outer diameter D , total length L , wall thickness t_1 for the cylindrical section, and a bottom thickness t_2 . The explosive charge, composed of C4, is housed within the casing and defined by diameter d and height l .

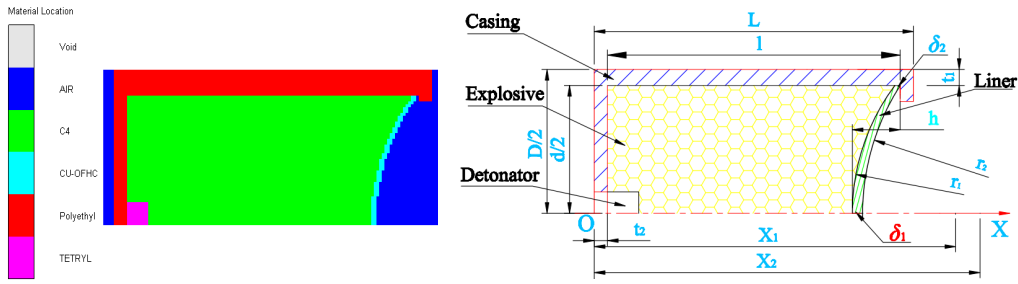


Fig. 1. Simulation model of the EFP warhead in Ansys Autodyn

To define the structural parameters of the warhead model under investigation, it was necessary to specify not only the device caliber D and the explosive charge diameter d , but also a set of preliminary design inputs. According to references [2, 4, 6], the studies have proposed recommended thickness ranges for uniform liners based on the liner diameter. However, there has been little in-depth research on non-uniform liners, especially regarding the acceptable range of top-to-edge thickness ratios and their relation to the overall liner diameter. Based on these sources, the present study selects liner top thickness values within the range of $0.02d$ to $0.07d$. The geometric parameters for each configuration are summarized in Table 1.

Among the configurations analyzed in the simulations, a liner top thickness of $\delta_1 = 2 \text{ mm}$ ($\delta_1/d \approx 0.044$) was chosen for experimental testing. This value lies within the optimal range of 0.04 to 0.05 times the liner diameter, as indicated by simulation results and previous studies [2, 5, 6]. This selection ensures that the test EFP is formed under realistic conditions to provide good warhead shape, stable flight path, and effective penetration. It is also suitable for actual production and testing.

The Ansys Autodyn software is used to simulate the formation of the EFP and its interaction with steel targets. The parameters obtained from the EFP formation simulation served as input data for simulating EFP impact on steel plate targets. Due to the axial

symmetry and to reduce the computation time, the problem model used is a 2D symmetric model. The casing, liner, explosive, and air were modeled with a Eulerian grid, using a cell size of $0.25 \text{ mm} \times 0.25 \text{ mm}$. Flow-out boundary conditions were applied to all computational domain boundaries except for the symmetry axis. The geometric model setup, including element selection, mesh sizing, geometry creation, material assignment, and gauge placement, was conducted in the Autodyn-2D environment [7–10].

Table 1. Geometric parameters to evaluate the influence of top liner thickness on EFP performance

Parameters	Unit	Type					
		1	2	3	4	5	6
D	mm			54			
d	mm			45.2			
L	mm			59.24			
l	mm			54.24			
t_1	mm			4.4			
t_2	mm			2.5			
h	mm			9.04			
δ_1	mm	0.904	1.356	1.808	2.26	2.712	3.164
δ_2	mm	0.452	0.678	0.904	1.13	1.356	1.582
X_1	mm	82.491	83.183	83.917	84.701	85.539	86.437
X_2	mm	84.821	86.893	89.197	91.777	94.693	98.024
R_1	mm	34.031	34.723	35.457	36.241	37.079	37.976
R_2	mm	35.457	37.077	38.929	41.057	43.521	46.4
δ_1/d		0.02	0.03	0.04	0.05	0.06	0.07

2.2. Material Model and Parameters

The plastic explosive C4 is modeled as an ideal elastoplastic material that follows the Mises yield criterion. Upon detonation, C4 transitions into a gaseous state and is described using the Jones-Wilkins-Lee (JWL) equation of state. In this model, the detonation product pressure p is a function of the relative volume V and the specific internal energy E .

$$p = A \left(1 - \frac{W}{R_1 V} \right) e^{-R_1 V} + B \left(1 - \frac{W}{R_2 V} \right) e^{-R_2 V} + \frac{WE}{V}, \quad (1)$$

where W, A, B, R_1, R_2 are experimental constants, with values in Table 2 [7–9].

The casing of the warhead is made of polyethylene plastic. Under explosive loading, the material undergoes significant volumetric and shape deformation. Therefore, the Shock equation of state is used to describe its behavior.

Table 2. Values of the parameters in the JWL equation of state for C4 explosive

W	A, GPa	B, GPa	R_1	R_2	$D, \text{m/s}$	$\rho, \text{g/cm}^3$	$E, \text{J/m}^3$
0.25	0.60977	0.01295	4.5	1.4	8193	1.601	9×10^9

Table 3. Values of the parameters in the Shock equation of state for polyethylene plastic

$\rho, \text{g/cm}^3$	Γ	$C_1, \text{cm}/\mu\text{s}$	S_1	$C_2, \text{cm}/\mu\text{s}$	S_2
0.915	1.64	0.2901	1.481	0	0

The liner is usually made of red copper M1 described by the modified Johnson-Cook (MJC) elastic-plastic model [7–9].

$$\sigma_c = (A + B\gamma_p^n) \left(1 + C \ln \left(\frac{\gamma^*}{\gamma_\bullet^*} \right) + D \left(\frac{\gamma^*}{\gamma_l^*} \right)^k \right) (1 - T_\sigma^m), \quad (2)$$

where σ_c is the dynamic yield stress; A, B, C, D, n, m and k are constants of the material determined experimentally; γ_p is the plastic strain; γ^* is the plastic strain rate; γ_\bullet^* is the reference value for the plastic strain rate; γ_l^* is the reference strain rate characterizing the transition between the thermally activated and viscous regimes; $T_\sigma = \frac{T - T_{ref}}{T_{melt} - T_{ref}}$; T is the instantaneous temperature; T_{ref} is the initial temperature; and T_{melt} is the melting temperature of the material. The OFHC copper liner was modeled using the MJC model, with the hardening constant increased from 0.292 GPa to 0.321 GPa ($\approx 10\%$) to prevent plastic instability at strain rates of $10^3 \div 10^6 \text{ s}^{-1}$. The Steel 1006 target was modeled using the standard JC model. Material parameters are given in Table 4.

To describe the equation of state of air in mathematical simulation, we use the ideal gas equation of state in gamma form [11].

$$p = \rho(\varepsilon - 1)E \quad (3)$$

where $\varepsilon = 1.4$, $\rho = 1.225 \text{ kg/m}^3$, and $E = 2.5 \times 10^5 \text{ J/kg}$ [11].

During the penetration process, the Lagrangian mesh is applied to both the EFP and the target. The simulation results of the EFP formation process using the Eulerian method are used to determine the EFP parameters. The target material is a sheet of steel described in the software as Steel 1006 with a width of 200 mm and a thickness of 30 mm. The equation of state for the target material is the Shock equation of state, while its strength and failure models are the Johnson-Cook models [12].

The simulation model of the impact process between the EFP and the steel target is shown in Fig. 2. Both EFP and target parts are modeled using 0.25 mm rectangular elements.

Table 4. Parameter values for the elastic-plastic models

Parameters	CU-OFHC	Steel 1006
Equation of state	Linear	Shock
Density (kg/m^3)	8960	7830
Melting temperature (K)	1356	1811
Strength model	MJC	JC
Yield stress A (GPa)	0.09	0.35
Hardening constant B (GPa)	0.3212	0.275
Strain rate constant C	0.025	0.022
Hardening exponent n	0.31	0.36
Thermal softening exponent m	1.09	1

Table 5. Values of the Johnson-Cook failure model parameters

D_1	D_2	D_3	D_4	D_5
0.05	4.22	-2.73	0.0018	0.55

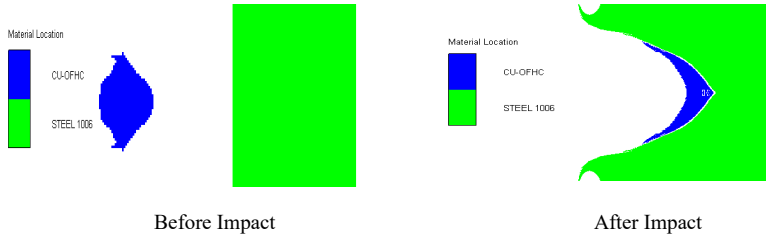


Fig. 2. Simulation of the penetration process of the EFP into the steel plate

3. EXPERIMENT

The formation and penetration process of the EFP was studied using both numerical simulations on Ansys Autodyn software and experimental methods. The obtained results, including the EFP's velocity, shape, hole diameter, and penetration depth upon impact with a 20 mm steel target, were compared.

3.1. Explosively Formed Projectiles and Experimental Target

For experimental validation, a liner with a top thickness of $\delta_1 = 2$ mm was chosen. The corresponding geometry and dimensions of this configuration are provided in Table 1. The forming liner is M1 copper. The shell is made of polyethylene plastic. The explosive charge is C4 plastic explosive. A No. 8 electric detonator is used to detonate

the EFPW. The target material is 45# steel. The target plate, shown in Fig. 3, was 20 mm thick, 500 mm wide, and 500 mm long.



Fig. 3. The EFPW and steel target

3.2. Experimental Setup

To validate the numerical model, an experimental test was conducted using a warhead with a liner top thickness of $\delta_1 = 2$ mm ($\delta_1/d \approx 0.044$), selected based on the optimal range identified in the simulation, with three samples tested to estimate the experimental variation [2, 12]. As illustrated in Fig. 4, the EFP warhead was mounted horizontally, with a 20 mm thick 45# steel plate positioned 3 meters downstream to serve as the target. An electronic timer (UTC8) placed 2 meters from the warhead was used to record the projectile's velocity. Following impact, the diameter and depth of the penetration hole on the target plate were measured to evaluate the EFP's terminal performance and compare it with the simulated results for Types 3 and 4.

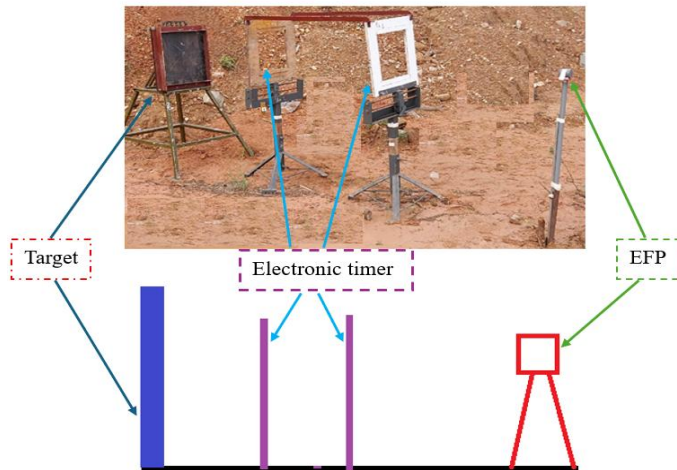


Fig. 4. Experimental setup for measuring EFP velocity and penetration depth

3.3. Experimental results

After the static blasting of the test specimens, the dimensions of the through-holes on the steel plate were measured to determine their diameter and depth, as shown in Fig. 5.

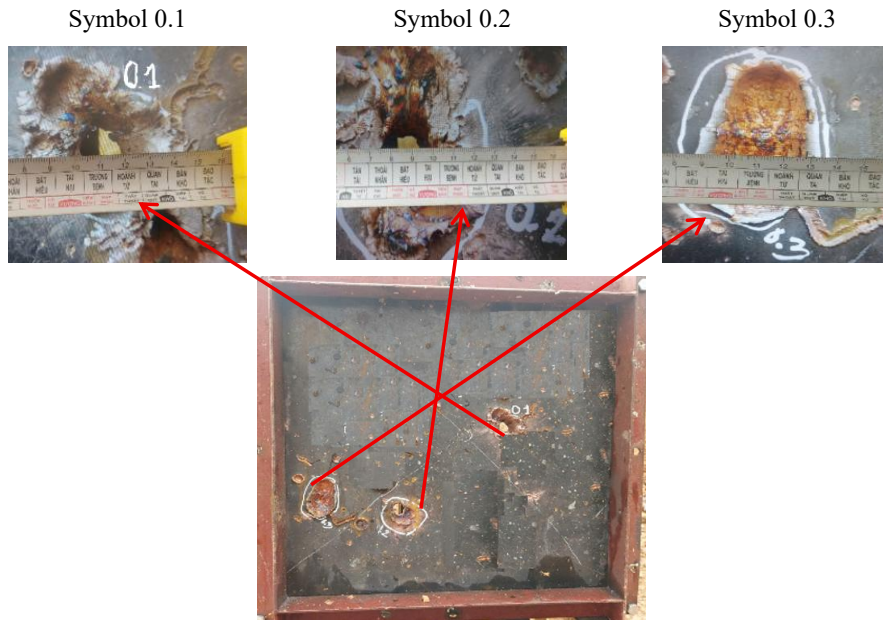


Fig. 5. Experimental results

The results for EFP velocity (V), hole diameter (W_h), and hole depth (D_h) from the tests are shown in Table 6.

Table 6. EFP velocity and penetration results on steel target

Type with $\delta_1 = 2 \text{ mm}$ ($\delta_1/d \approx 0.044$)			
Symbol	0.1	0.2	0.3
$V \text{ (m/s)}$	2278	2150	1859
$V_{Ag} \text{ (m/s)}$		2096	
$W_h \text{ (mm)}$	36	37	40
$W_{h.Ag} \text{ (mm)}$		37.7	
$D_h \text{ (mm)}$	20	20	18

4. RESULTS AND DISCUSSION






Table 7 presents the results of the investigation on the impact of the top thickness liner on EFP formation in EFPW at time $t = 0.8$ ms for all EFP warhead structures with the parameters listed in Table 1.


























4.1. Shape of EFP

The formation behavior of an EFP is strongly influenced by the top thickness of the liner. During the initial stage of detonation (approximately 0.1 to 0.3 milliseconds), shock waves generated by the explosive charge first impact the center of the liner, initiating a collapse process. This causes the liner material to accelerate and flow along the axis of symmetry to form the projectile. The top thickness of the liner, δ_1 , plays a decisive role in controlling the collapse speed, as well as the direction and momentum of the material flow during projectile formation. A thinner top results in faster collapse and higher acceleration, while a thicker top delays the collapse due to greater mass and resistance to deformation. These differences directly affect the final shape, structural coherence, and flight stability of the projectile.

Table 7 shows the evolution of projectile morphology for δ_1/d ranging from 0.02 to 0.07. At lower ratios ($\delta_1/d \leq 0.03$), the top collapses rapidly due to minimal resistance, causing excessive radial flow and the formation of blunt projectiles. These shapes exhibit poor aerodynamic performance and are prone to yaw during flight. Conversely, for $\delta_1/d \geq 0.06$, the increased mass at the top introduces high inertia, resulting in incomplete collapse and hollow-core formation near the tail region, which is a known instability during EFP formation. The optimal morphologies are observed for δ_1/d values between 0.03 and 0.05, where the top collapses smoothly, maintaining axisymmetric flow and producing long, pointed projectiles with solid bodies and high structural integrity. These characteristics are critical for maintaining aerodynamic stability and enhancing penetration capability [13].

Table 7. Shape of EFP at specific times and displacements

Time (ms)		0.1	0.3	0.5	0.8
Type 1 $V_{EFP} = 2887$ m/s $E_{kin} = 32.14$ kJ					
	Displacement (mm)	348	977	1594	2378

Time (ms)		0.1	0.3	0.5	0.8
Type 2 $V_{EFP} = 2470 \text{ m/s}$ $E_{kin} = 39.31 \text{ kJ}$					
	Displacement (mm)	294	801	1304	2051
Type 3 $V_{EFP} = 2110 \text{ m/s}$ $E_{kin} = 36.83 \text{ kJ}$					
	Displacement (mm)	257	688	1116	1752
Type 4 $V_{EFP} = 1827 \text{ m/s}$ $E_{kin} = 36.52 \text{ kJ}$					
	Displacement (mm)	231	602	971	1522
Type 5 $V_{EFP} = 1620 \text{ m/s}$ $E_{kin} = 33.78 \text{ kJ}$					
	Displacement (mm)	210	540	868	1356
Type 6 $V_{EFP} = 1431 \text{ m/s}$ $E_{kin} = 32.34 \text{ kJ}$					
	Displacement (mm)	193	483	772	1203

4.2. Velocity of EFP

The tip velocity of the EFP is significantly influenced by the top thickness of the liner, denoted as δ_1/d . As this ratio increases from 0.02 to 0.07, a clear and consistent decrease in projectile velocity is observed.

At $\delta_1/d = 0.02$ (Type 1), the highest velocity is achieved at 2887 m/s, owing to the thin liner's low mass and reduced resistance to collapse. When the ratio increases to 0.03 (Type 2), the velocity drops to 2470 m/s, representing a 14.4% decrease. For $\delta_1/d = 0.04$ (Type 3), the velocity continues to fall to 2110 m/s, and then to 1827 m/s at $\delta_1/d = 0.05$ (Type 4). At $\delta_1/d = 0.06$ (Type 5) and 0.07 (Type 6), the projectile velocities decrease further to 1620 m/s and 1431 m/s, respectively.

In summary, as the liner becomes thicker, the projectile velocity declines due to the increased inertia of the liner material, which resists rapid acceleration. This trend is clearly depicted in Fig. 6, where the projectile velocity decreases progressively with increasing δ_1/d ratio. The graph confirms that the highest velocity is achieved at $\delta_1/d = 0.02$, followed by a steady decline as the top thickness increases. Thin liners favor high-speed projectile formation, but this speed must be balanced with other performance parameters, such as energy and structural coherence.

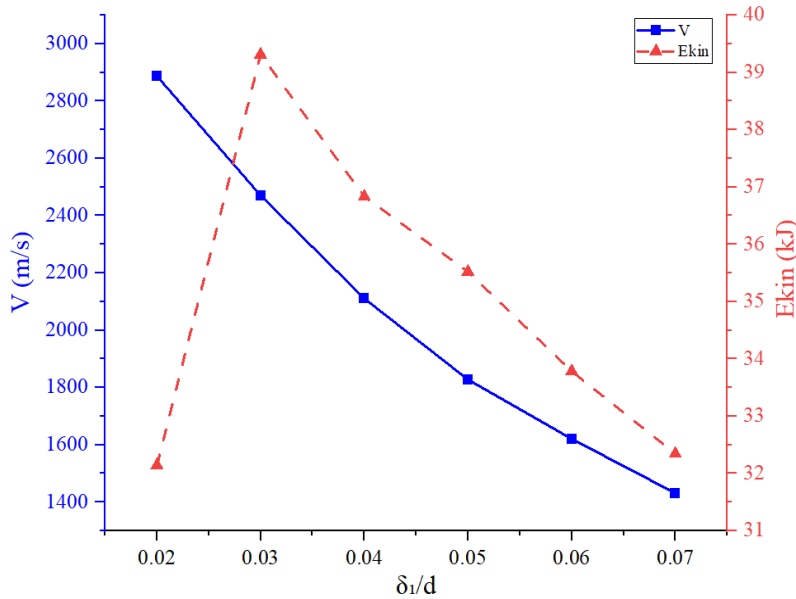


Fig. 6. Variation of EFP velocity and kinetic energy with liner top thickness

4.3. Kinetic Energy of EFP

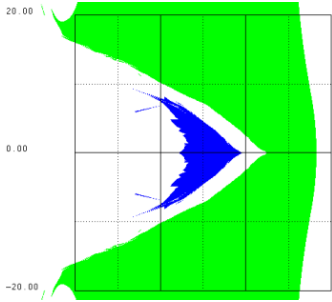
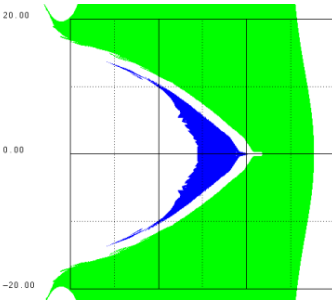
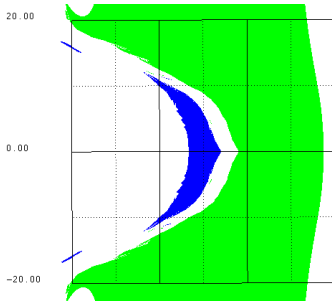
While velocity decreases with increasing δ_1/d , the kinetic energy of the EFP exhibits a non-linear trend. It initially increases, reaches a peak, and then gradually declines as the liner becomes thicker.

At $\delta_1/d = 0.02$ (Type 1), the kinetic energy is 32.14 kJ. This relatively low value, despite the high velocity, is due to the small mass of the liner. When δ_1/d increases to 0.03

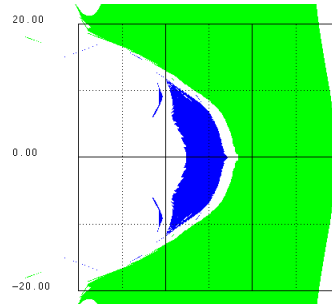
(Type 2), the kinetic energy rises sharply to 39.31 kJ, reflecting an optimal combination of liner mass and acceleration. However, as δ_1/d increases further to 0.04 and 0.05, the kinetic energy drops slightly to 36.83 kJ and 36.52 kJ, respectively. At $\delta_1/d = 0.06$ (Type 5), it decreases to 33.78 kJ and returns to 32.34 kJ at $\delta_1/d = 0.07$ (Type 6).

These results demonstrate that the most efficient transfer of energy from the explosive to the projectile occurs when δ_1/d is approximately 0.03. Fig. 6 clearly illustrates this: the conversion of explosive energy into the EFP's kinetic energy peaks at a δ_1/d ratio of about 0.03. Below this value, the projectile mass is too small to store substantial energy; above it, the increased mass impedes acceleration, and a larger share of the energy is dissipated as plastic deformation of the liner.

Table 8. EFP penetration process with different liner top thicknesses

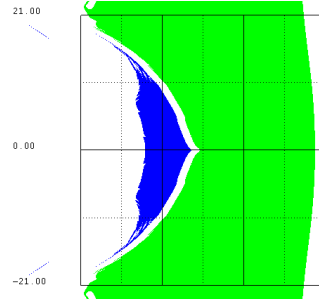
Type 1		Hole diameter $d_h = 34$ mm; Hole depth $b = 24$ mm
Type 2		Hole diameter $d_h = 37$ mm; Hole depth $b = 26$ mm
Type 3		Hole diameter $d_h = 39$ mm; Hole depth $b = 23$ mm

Type 4



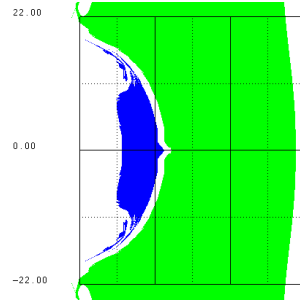
Hole diameter $d_h = 40$ mm;
Hole depth $b = 19$ mm

Type 5



Hole diameter $d_h = 42$ mm;
Hole depth $b = 15$ mm

Type 6



Hole diameter $d_h = 44$ mm;
Hole depth $b = 12$ mm

4.4. Penetration Process

Following formation, the EFP impacts a 45# steel target plate with a thickness of 30 mm. As illustrated in Fig. 7, the target material experiences significant compressive and shear stresses, which constitute the primary failure mechanisms during interaction with the EFP. A combined tensile-compressive stress distribution is observed at both the front and rear surfaces of the target. As penetration progresses, tensile stresses increasingly dominate, particularly at the edges of the shear zone due to pronounced material elongation [4, 14]. The reflection of transverse waves at the rear surface, along with continuous projectile penetration, further accelerates target degradation. Two distinct active zones are identified: a compressive zone near the front surface, where compressive failure prevails; and a tensile zone near the rear surface, characterized by tensile-induced damage [4, 14–16]. With increasing penetration depth, resistance to projectile motion intensifies, resulting in an expanding damage region within the target.

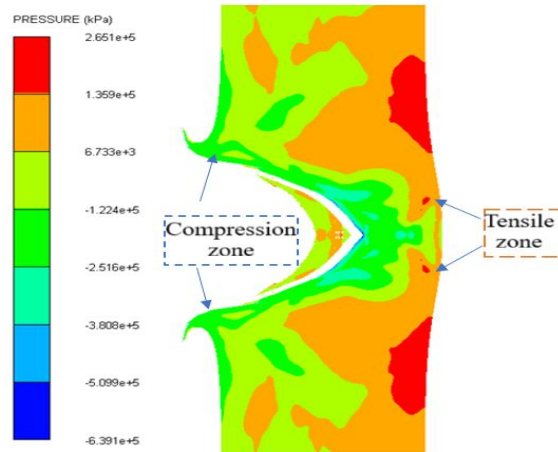


Fig. 7. Steel target plate subjected to EFP impact

The final effectiveness of the EFP is evaluated through its penetration into a steel target, specifically the diameter and depth of the impact cavity. The results indicate a strong dependence on liner top thickness, as shown in Table 8.

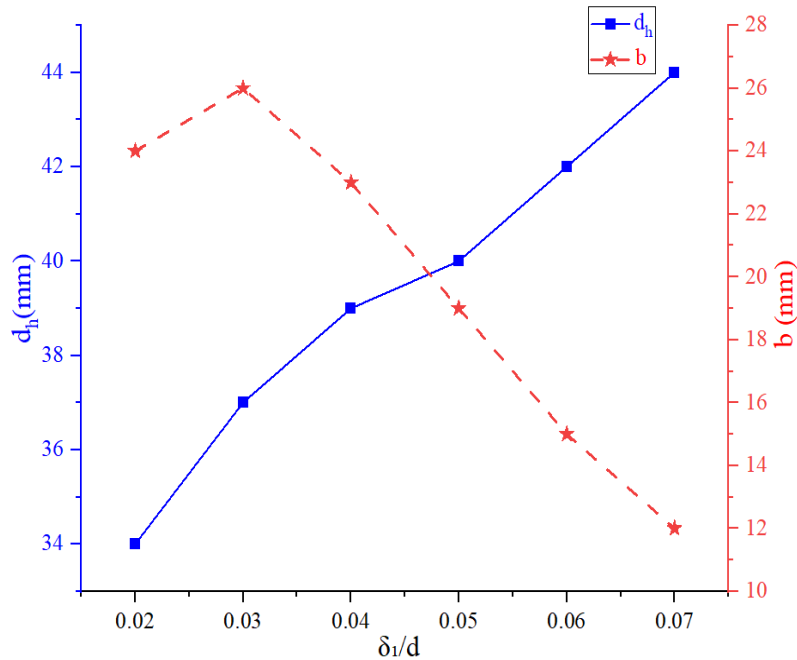


Fig. 8. Effect of liner top thickness on hole diameter and hole depth

At $\delta_1/d = 0.02$ (Type 1), the EFP penetrates to a depth of 24 mm with a hole diameter of 34 mm. Increasing δ_1/d to 0.03 (Type 2) reduces penetration depth slightly to 26 mm,

but increases the diameter to 37 mm. At $\delta_1/d = 0.04$ (Type 3), the depth declines to 23 mm, while the diameter expands to 39 mm. Further increases to $\delta_1/d = 0.05$ and 0.07 (Types 4 and 6) result in continued reductions in penetration depth-down to 15 mm and 12 mm, respectively while hole diameters reach 42 mm and 44 mm.

These trends confirm that thicker liners produce wider but shallower craters, due to the formation of heavier, slower projectiles with poorer axial momentum. In contrast, thinner liners generate narrower but deeper cavities, which are more favorable for perforation-focused applications. This behavior is clearly reflected in Fig. 8, which shows an inverse relationship between penetration depth and hole diameter as δ_1/d increases.

4.5. Experimental Validation

To validate the simulation results under realistic conditions, an experimental trial was conducted using a liner with a top thickness of $\delta_1 = 2$ mm and a base thickness of $\delta_2 = 1$ mm, corresponding to $\delta_1/d \approx 0.044$. This configuration was deliberately selected based on its location within the optimal δ_1/d range (0.03–0.05) identified through simulation, where projectile velocity, energy transfer, and penetration efficiency reached favorable levels. $\delta_1/d \approx 0.044$ thickness was chosen to validate the numerical model at an interpolated value between two adjacent cases (Type 3 and 4), as illustrated clearly in the velocity and penetration graphs. This approach not only reflects a practical design for fabrication but also enhances the robustness of the validation by confirming the predictive accuracy of the simulation across intermediate values. The experiment yielded a tip velocity of 2096 m/s, penetration depth of 20 mm, and cavity diameter of 37.7 mm. These results are within the predicted range of neighboring simulation cases, as shown in Table 9.

Table 9. Comparison of simulation and experimental results

Metric	Type 3 ($\delta_1/d = 0.04$)	Type 4 ($\delta_1/d = 0.05$)	Experiment ($\delta_1/d = 0.044$)
EFP velocity (m/s)	2110	1827	2096
Hole diameter (mm)	40	42	37.7
Hole depth (mm)	19	15	> 20

The differences between simulation and experiment are within 5–10%, which are acceptable in light of experimental uncertainties, such as material inconsistencies, machining tolerances, and boundary effects. The selected test configuration, positioned between two modeled cases within the optimal simulation range, aligns closely with predicted trends. Its measured performance validates the reliability of the simulation model and

confirms that $\delta_1/d \approx 0.044$ design is both practical and effective for real-world EFP applications.

5. CONCLUSION

This study presented a combined numerical and experimental investigation into the influence of liner top thickness (δ_1) on the performance of explosively formed projectiles (EFP). The results showed that:

- Projectile velocity decreases as δ_1/d increases, due to higher liner mass and collapse resistance.

- Kinetic energy reaches its peak at $\delta_1/d \approx 0.03$, indicating the most efficient energy transfer from explosive to projectile.

- Penetration performance shows a trade-off: thinner liners yield greater depth, while thicker liners create wider but shallower cavities.

- Experimental validation is conducted at $\delta_1/d \approx 0.044$, a carefully chosen configuration within the optimal range determined by simulation with an acceptable error, consolidating the accuracy and applicability of the numerical model.

These findings provide valuable guidance for future EFP design and validate the use of numerical tools as effective predictors of real-world behavior.

FUNDING

This research received no specific grant from any funding agency in the public, commercial, or not-for-profit sectors.

DECLARATION OF COMPETING INTEREST

The authors declare that they have no known competing financial interests or personal relationships that could have appeared to influence the work reported in this paper.

REFERENCES

- [1] D. Cardoso and F. Teixeira-Dias. Modelling the formation of explosively formed projectiles (EFP). *International Journal of Impact Engineering*, **93**, (2016), pp. 116–127. <https://doi.org/10.1016/j.ijimpeng.2016.02.014>.
- [2] D. Yang and J. Lin. Numerical investigation on the formation and penetration behavior of explosively formed projectile (EFP) with variable thickness liner. *Symmetry*, **13**, (2021). <https://doi.org/10.3390/sym13081342>.

- [3] V. M. Do, D. T. Tran, X. S. Bui, H. Q. Pham, H. N. Pham, P. Konečný, T. A. Hoang, and D. T. To. Influence of liner curvature radiuses on the formation process and penetration capability of explosively formed projectile. In *The 2025 International Conference on Military Technologies (ICMT)*, IEEE, (2025), pp. 1–7. <https://doi.org/10.1109/icmt65201.2025.11061281>.
- [4] H. Q. Pham, V. M. Do, D. T. Tran, X. S. Bui, H. N. Pham, and D. T. To. Experimental and numerical study on the influence of liner height on explosively formed projectiles. *Journal of Advances in Military Technology*, **20**, (2025), pp. 211–225. <https://doi.org/10.3849/aimt.01961>.
- [5] M. Salkičević. Numerical simulations of the formation behavior of explosively formed projectiles. *Defense and Security Studies*, **3**, (2022), pp. 1–14. <https://doi.org/10.37868/dss.v3.id183>.
- [6] J. Wu, J. Liu, and Y. Du. Experimental and numerical study on the flight and penetration properties of explosively-formed projectile. *International Journal of Impact Engineering*, **34**, (2007), pp. 1147–1162. <https://doi.org/10.1016/j.ijimpeng.2006.06.007>.
- [7] H. Couque and R. Boulanger. EFP simulations with Johnson-Cook models. In *The 23rd International Symposium on Ballistics*, Tarragona, Spain, (2007).
- [8] H. Couque, R. Boulanger, and F. Bornet. A modified Johnson-Cook model for strain rates ranging from 10^3 to 10^5 s⁻¹. *Journal de Physique IV (Proceedings)*, **134**, (2006), pp. 87–93. <https://doi.org/10.1051/jp4:2006134015>.
- [9] G. Hussain, A. Hameed, J. G. Hetherington, P. C. Barton, and A. Q. Malik. Hydrocode simulation with modified Johnson-Cook model and experimental analysis of explosively formed projectiles. *Journal of Energetic Materials*, **31**, (2013), pp. 143–155. <https://doi.org/10.1080/07370652.2011.606453>.
- [10] G. R. Johnson and W. H. Cook. Fracture characteristics of three metals subjected to various strains, strain rates, temperatures and pressures. *Engineering Fracture Mechanics*, **21**, (1985), pp. 31–48. [https://doi.org/10.1016/0013-7944\(85\)90052-9](https://doi.org/10.1016/0013-7944(85)90052-9).
- [11] ANSYS, Inc. *Ansys Autodyn user's manual*. Release 19.0, p. 512, (2021).
- [12] M. R. Vaziri, M. Salimi, and M. Mashayekhi. A new calibration method for ductile fracture models as chip separation criteria in machining. *Simulation Modelling Practice and Theory*, **18**, (2010), pp. 1286–1296. <https://doi.org/10.1016/j.simpat.2010.05.003>.
- [13] L. P. Orlenko. *Physics of explosion and impact*. Fizmatlit, Moscow, 2nd edition, (2008). (in Russian).
- [14] N. T. Khiem and P. T. Hang. A novel damage index extracted from frequency response of cracked Timoshenko beam subjected to moving harmonic load. *Vietnam Journal of Mechanics*, **44**, (2022), pp. 280–291. <https://doi.org/10.15625/0866-7136/17546>.
- [15] M. V. Pham, M. N. Nguyen, and T. Q. Bui. A staggered local damage model for fracture analysis in bi-material structures. *Vietnam Journal of Mechanics*, **46**, (2024), pp. 217–228. <https://doi.org/10.15625/0866-7136/21007>.
- [16] N. H. Hao. Forming limit prediction of advanced high-strength steels (AHSS) using an enhanced ductile damage model. *Vietnam Journal of Mechanics*, **47**, (2025), pp. 142–153. <https://doi.org/10.15625/0866-7136/22179>.